SHIP PRODUCTION COMMITTEE
FACILITIES AND ENVIRONMENTAL EFFECTS
SURFACE PREPARATION AND COATINGS
DESIGN/PRODUCTION INTEGRATION
HUMAN RESOURCE INNOVATION
MARINE INDUSTRY STANDARDS
WELDING
INDUSTRIAL ENGINEERING
EDUCATION AND TRAINING

November 1993
NSRP 0408

THE NATIONAL SHIPBUILDING RESEARCH PROGRAM

1993 Ship Production Symposium

Paper No. 20: Prediction of the Low Cycle Fatigue Life of HY-100 Undermatched Welds in Marine Structure

U.S. DEPARTMENT OF THE NAVY
CARDEROCK DIVISION,
NAVAL SURFACE WARFARE CENTER

Report Documentation Page

Form Approved
OMB No. 0704-0188

1. REPORT DATE	2. REPORT TYPE	3. DATES COVERED
NOV 1993	**N/A**	**-**

4. TITLE AND SUBTITLE	5a. CONTRACT NUMBER
The National Shipbuilding Research Program, 1993 Ship Production Symposium Paper No. 20: Prediction of the Low Cost Fatigue Life of Hy-100 Undermatched Welds in Marine Structure	5b. GRANT NUMBER
	5c. PROGRAM ELEMENT NUMBER
6. AUTHOR(S)	5d. PROJECT NUMBER
	5e. TASK NUMBER
	5f. WORK UNIT NUMBER
7. PERFORMING ORGANIZATION NAME(S) AND ADDRESS(ES) **Naval Surface Warfare Center CD Code 2230 - Design Integration Tower Bldg 192 Room 128 9500 MacArthur Blvd Bethesda, MD 20817-5700**	8. PERFORMING ORGANIZATION REPORT NUMBER
9. SPONSORING/MONITORING AGENCY NAME(S) AND ADDRESS(ES)	10. SPONSOR/MONITOR'S ACRONYM(S)
	11. SPONSOR/MONITOR'S REPORT NUMBER(S)

12. DISTRIBUTION/AVAILABILITY STATEMENT
Approved for public release, distribution unlimited

13. SUPPLEMENTARY NOTES

14. ABSTRACT

15. SUBJECT TERMS

16. SECURITY CLASSIFICATION OF:			17. LIMITATION OF ABSTRACT	18. NUMBER OF PAGES	19a. NAME OF RESPONSIBLE PERSON
a. REPORT	b. ABSTRACT	c. THIS PAGE			
unclassified	**unclassified**	**unclassified**	**SAR**	**14**	

Standard Form 298 (Rev. 8-98)
Prescribed by ANSI Std Z39-18

DISCLAIMER

These reports were prepared as an account of government-sponsored work. Neither the United States, nor the United States Navy, nor any person acting on behalf of the United States Navy (A) makes any warranty or representation, expressed or implied, with respect to the accuracy, completeness or usefulness of the information contained in this report/ manual, or that the use of any information, apparatus, method, or process disclosed in this report may not infringe privately owned rights; or (B) assumes any liabilities with respect to the use of or for damages resulting from the use of any information, apparatus, method, or process disclosed in the report. As used in the above, “Persons acting on behalf of the United States Navy” includes any employee, contractor, or subcontractor to the contractor of the United States Navy to the extent that such employee, contractor, or subcontractor to the contractor prepares, handles, or distributes, or provides access to any information pursuant to his employment or contract or subcontract to the contractor with the United States Navy. ANY POSSIBLE IMPLIED WARRANTIES OF MERCHANTABILITY AND/OR FITNESS FOR PURPOSE ARE SPECIFICALLY DISCLAIMED.

0408

THE NATIONAL SHIPBUILDING RESEARCH PROGRAM

1993

SHIP PRODUCTION SYMPOSIUM

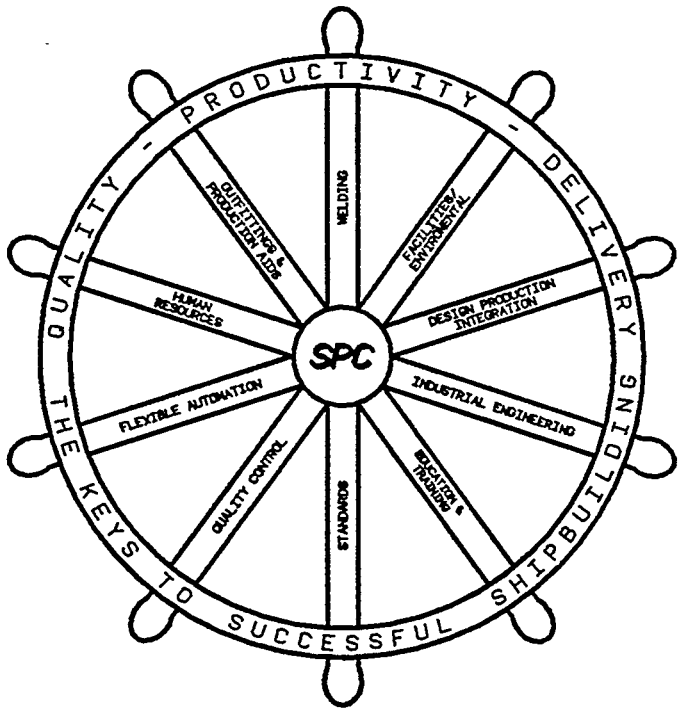

Sponsored by the Hampton Roads Section
Society of Naval Architects & Marine Engineers

CENTENNIAL
1893-1993

Williamsburg Virginia, November 1-4, 1993

CENTENNIAL

The National Shipbuilding Research Program
1993 Ship Production Symposium
Sponsored by the Hampton Roads Section SNAME

Prediction of the Low Cycle Fatigue Life of HY-1OO Undermatched Welds in Marine Structures

R S. Shaw (V), K C. Wang (V) and M. J. KIeiuowski (V)-Concurrent Technologies, PA

ABSTRACT

Finite element and analytical models are used in this study to predict the low cycle fatigue life of undermatched (lower yield strength) weldments of HY-100 steel. The objective was to determine the feasibility of replacing conventional overmatched welds in marine structures. Fatigue tests were performed on standard, smooth specimens, notched cylindrical specimens and a four point bend test on a full scale butt beam specimen. Numerical analyses were conducted using finite elements, with a two surface plasticity algorithm to simulate the cyclic behavior of the individual materials. The stress and strain concentrations at the notches were also evaluated using two analytical models: the Neuber and Glinka relations. The finite element predictions compared well with experimental data, and produced detailed predictions of the strain distributions, which were then used to assess the crack initiation life. Glinka's relation demonstrated superior predictive capabilities for local strains over Neuber's relation.

INTRODUCTION

In the past, overmatched weldments have been successfully used in the design of high strength steel naval structures. The high yield strength of the weld metal, in comparison to that of the base metal, ensures adequate strength and prevents the development of high strains in the weldment. Also, the performance of overmatched welds under low cycle fatigue loading conditions has proven to be adequate. However, for high strength steels, such as HY-1OO and above, the welding process envelope is severely restricted. For this reason, and for cost efficiency, undermatched welds have recently been considered in applications. Some of the major concerns that need to be addressed before actually using. the undermatched welds are their low cycle fatigue properties, their fracture resistance when subjected to both high static loads or dynamic loads, and the static strength of the weld during localized yielding.

For the past twenty years, numerous small scale and full scale overmatched weldments of HY series steels were tested, and the studies concluded that their fatigue crack initiation life generally fell into the same envelope. The scatter of the crack initiation of the weldments was usually more significant than that of the base metals (1,2). This is mainly because of imbedded defects, such as porosity, inclusion, and under-cut produced during welding. Local strains encountered in undermatched weldments could vary considerably from their overmatched counterparts. This is not only due to the difference in material properties, but also as a result of the different heat treatments applied during welding. In this study, the low cycle fatigue behavior of undermatched welds of HY-1OO steel has been invemigatcd.

Since low cycle fatigue is a local strain-dominated phenomena, the prediction of the local stress-strain response is crucial. Determining the notch root strain is usually difflcult, since the effect of the notch root constraint by the surrounding elastic material is quite significant. Several approaches were evaluated for their effectiveness in predicting the initiation of low cycle fatigue cracks at welded structural details. Analytical models such as Neuber's Rule (3) and Glinka's method (4), as well as computationally intensive two- and three-dimensional finite element models, were evaluated against experimental data. The analytical models are based on either plane stress or plane strain situations, so that when three-dimensional effects are present, the local strains predicted by these methods usually yield unsatisfactory results. Three-dimensional finite element models are more accurate in this respect.

Experiments consisted of fatigue tests on standard smooth cylindrical specimens, used to generate the baseline weld metal fatigue data. The specimens were oriented both along and transverse to the welding direction, so that the anisotropy of the weld could be investigated. Cylindrical notched specimens of weld metal, with different notch root radii to produce different notch root constraints, were also tested under cyclic loading conditions. Finally, a butt beam fatigue specimen, machined from a double-V joint welded plate, was subjected to a four point bend cyclic loading. This specimen consisted of base and weld metal, as well as the heat affected zone (HAZ), with a notch machined in the weld through the width of the plate.

The object of this study was to generate baseline low cycle fatigue data for weld metal to be used as the basic material property data for the numerical and analytical models. These models could then be utilized to predict notch root strains and cycles to crack initiation in structural components of various

geometries. Some initial experimental and modeling work for this study appears in (5,6).

TECHNICAL APPROACH

Low cycle fatigue crack initiation depends primarily on the strain range experienced at the crack initiation site. The accurate prediction of the local strain response is therefore most important. The basic concept of using the local approach for the crack initiation stage was outlined by Crews and Hardrath (7) in the "Companion Specimen Method - Equal Deformation Equal Life Concept." The main assumption in their method is that the notch root material and an unnotched specimen of the same material behave similarly, and show the same crack initiation life behavior. Therefore, the local stresses at the root of the notched specimen or component can be determined by first experimentally measuring the notch root strain and applying these local strains to the smooth specimen. The resulting stress measured from the smooth specimen will then, according to this concept, correspond to the stress at the notch root. In other words, a smooth specimen can be used to simulate the material stress-strain response and damage accumulation at the notch root of a notched component.

The basic concept outlined above has been used in this study. Several smooth specimens of weld metal were cycled between various strain ranges, and the number of cycles to crack initiation was established for each strain range. Crack initiation was assumed to occur when a significant drop in material stiffness was observed. This set of experiments served to establish both the elastic-plastic material properties, and the low cycle fatigue properties of the weld metal. Similar experiments were also conducted on HY-1OO specimens, and testing is currently in progress on the HAZ.

Following these tests, the elastic-plastic material properties were fed into finite element models of notched cylindrical and notched beam specimens. Cyclic loading of a stabilized loading cycle was simulated on the models. The predicted strain range at the notch root of the models was then compared with the "strain range versus number of cycles to crack initiation" curve established from the experiments on smooth specimens. The number of cycles to crack initiation, as predicted by the numerical notched models was extrapolated from this curve. Similarly, notch root strains evaluated from Neuber's and Glinka's analytical models were compared with the experimental curves, and the number of cycles to damage initiation was extrapolated.

In order to validate the numerical and analytical models, experimental fatigue tests were conducted on notched specimens, and the measured values were compared with the model predictions.

EXPERIMENTAL PROGRAM

The experimental program was divided into two parts. The first involved obtaining the basic material property data, namely the cyclic stress-strain response and the baseline crack initiation data. The second set of experiments were fatigue tests performed on notched specimens. The data obtained from these tests was used to validate the accuracy of the numerical and analytical models. The specimens used to generate the cyclic stress-strain curves, baseline crack initiation data and failure life were similar to those stipulated by ASTM E606 (8).

Testing of Hourglass Specimens

Smooth hourglass shaped specimens were manufactured transverse to and along the welding direction for the weld metal, and transverse to and along the rolling direction for the HY-1OO steel base metal. The minimum gage section diameter of the specimens was 6.4 mm (0.25 in), each machined with a fine finished surface. Figure la depicts the typical geometry of these specimens. The purpose of these tests was to obtain the material cyclic stress strain response. The reason for using hourglass shaped specimens was to minimize to the possibility of buckling during compression. This type of specimen can generally reach higher strain ranges than the smooth straight specimen (Figure lb), before buckling.

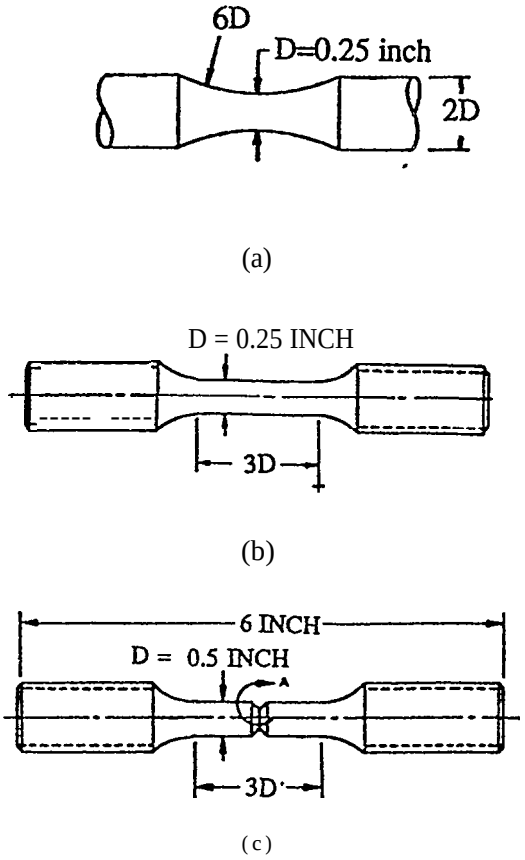

Figure 1. Schematic of (a) hourglass cyclic specimen, (b) cylindrical smooth fatigue specimen, (c) cylindrical notched fatigue specimen.

Incrementally increasing and decreasing strain controlled loading sequences were used, with the maximum strain reaching plus and minus 1.25 percent, A diametral displacement measurement gage was used to measure the deformations during cycling of the specimen. Poisson's ratio was measured as 0.295, and was used to calculate the axial cyclic stess-strain curve. A typical experimental loading curve for undermatched weld metal is shown in Figure 2. Comparisons were also made with HY-130, HY-80 and HY-NXI base metals. It was observed that the weld metal exhibited significant cyclic softening with a higher hardening exponent than its parent metal. There was little difference observed between the transverse or Iongitudinal cyclic stress-strain curves of either the base or the weld metal. The initial and stabilized cycles have been plotted in Figures 3 and 4 for the base and weld metal, respectively. Table I contains the average elastic modul measured from these tests.

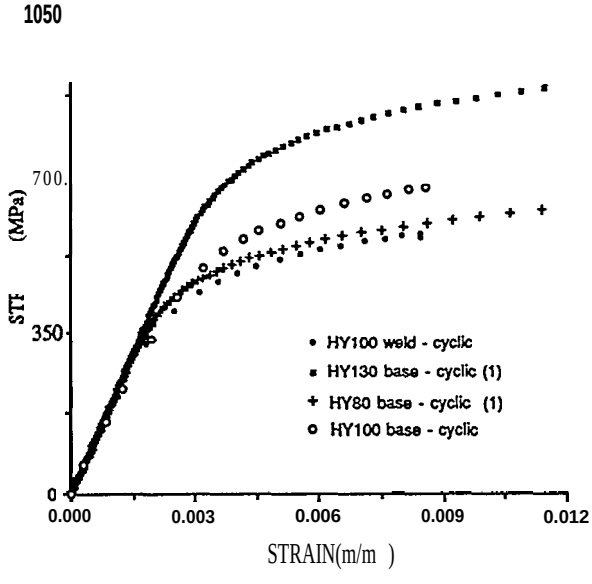

Figure 2. Stress-strain curves for weld metal, HY-1OO, HY-80 (1) and HY130 (1) Steel.

Material	First Cycle		Stabilized Cycle	
	Long. Mod. (GPa)	Trans. Mod. (GPa)	Long. Mod. (GPa)	Trans. Mod.
Base Metal	201.19	194.64	189.12	189.33
Weld Metal	203.81	206.98	188.43	205.81

Table I. Measured average values of elastic Young's modulus for HY-1OO base metal and weld metal.

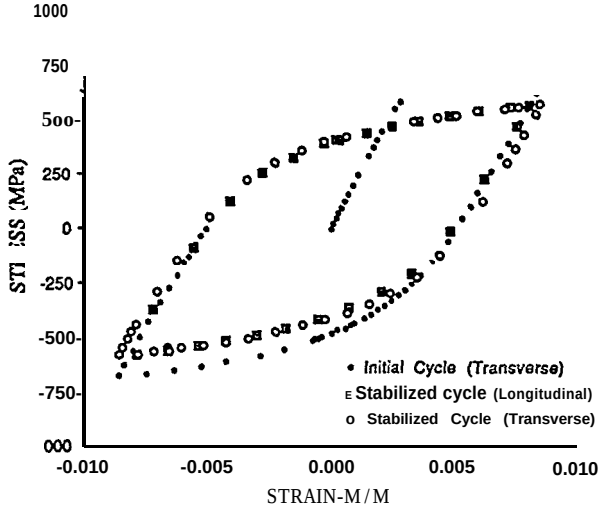

Figure 3. Initial and stabilized stress-strain hysteresis loops of the weld metal.

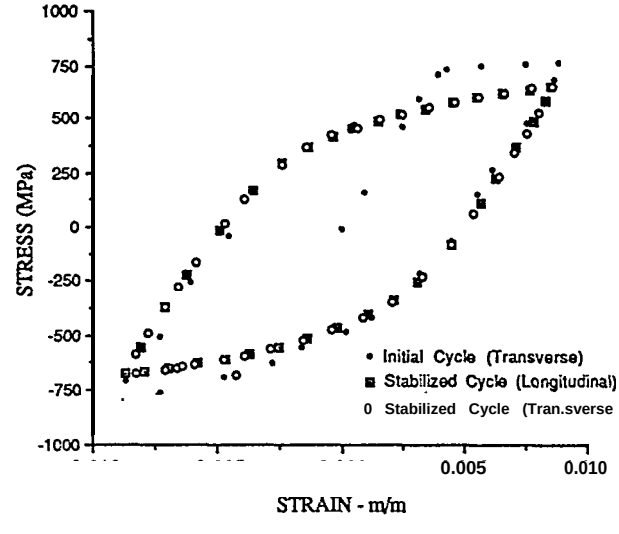

Figure 4. Initial and stabilized stress-strain hysteresis loops of HY-100 steel.

Testing of Smooth Fatigue Specimens

Smooth cylindrical tensile crack initiation fatigue specimens (Figure lb) with diameter 6.4 mm (0.25 in), were used to generate baseline weldment fatigue data. As before, specimens oriented transverse to and along the weld were considered to investigate the weldment anisotropy. Specimen surfaces were fine finished to avoid any artificial effect on their fatigue behavior. Strain control fully reversed loading ($R = {}^{6}min/{}^{a}max = -1$) was applied to all specimens. The load ranges were selected. from a nominal maximum

strain of 0.35 percent to 1.0 percent, such that the crack initiation or failure lives covered a range of approximately 1000 cycles to less than 50000 cycles. The cycle frequency used was 0.5 hertz. All tests were performed on computer-controlled servohydraulic tension-compression testing machines. The readings from the load cell and extensometer were recorded periodically. Crack initiation was defined to occur when the maximum load dropped significantly, indicating a drop in the stiffness of the specimen. Figure 5 shows a plot of the total strain range versus cycles to crack initiation for the weld metal. Also included are data for HY-80, HY-1OO, HY-130 base metal taken from reference (l).

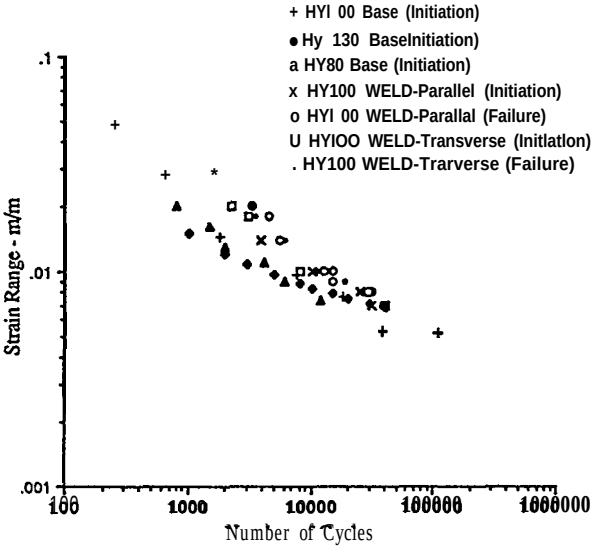

Figure 5. Total strain range vs. number of cycles to crack initiation or failure of HY-1OO welds. Data for HY-130 and HY-80 are from (l).

Testing of Notched Cylindrical Specimens

Testing of the notched specimens was performed using cylindrical specimens of weld metal with two different notch root radii, with the same notch depth. A schematic illustration of this type of specimen is shown in Figure lc. The specimen diameter is 12.7 mm (0.5 in) instead of 6.4 mm (0.25 in) so that the crack initiation and the failure could be defined more easily. For cylindrical notched specimens with 6.4 mm (0.25 in) diameter, crock initiation is usually difficult to detect before complete fracture occurs. The loading of the notched specimen was monitored using an extensometer, which was attached across the notch opening. The gage length of the extensometer was 25.4 mm (1.0 in) so that the recorded strains could be treated as remote strains. The notch root radii were 0.635 mm (0.025 in) for the type I notch, and 0.381 mm (0.015 in) for the type II notch. The notch depth was approximately 2.12 mm (0.0833 in), one-third of the radius. The notch root surfaces were also polished to have a fine finished surface. The loading was strain controlled, with R = -1.0 fully reversed load monitored by the extensometer, ranging from 0.15 to 0.35 percent strain amplitude. The crack initiation was assumed to occur when an abrupt drop was observed in the load sustained by the specimen.

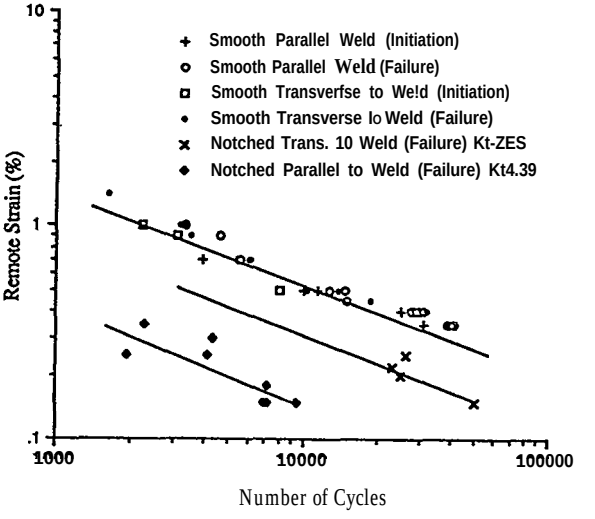

Figure 6. Comparison of the crack initiation life of smooth and notched specimens of HY-1OO weld metal.

As with the smooth specimens, all tests were performed on computer-controlled servohydraulic tension-compression testing machines. A comparison of the experimental crack initiation life between smooth and notched specimens appears in Figure 6.

Four Point Bend Test of a Full Scale Welded Beam

In order to assess the fatigue crack initiation life for a full scale welded component of HY-1OO steel, a four point bend fatigue specimen was welded and machined, and loaded with a bending moment with loading ratio R = O (zero to tension loading). This specimen used a double-V joint weld plate with a welded inclusion angle of approximately 60 degrees. The dimensions of the four point bend specimen were 0.58 m (23.0 in) by 0.127 m (5.0 in) by 0.051 m (2.0 in) (length x height x thickness). A small through notch with notch root radius 0.4 mm (0.0158 in), and notch depth 2.41 mm (0.095 in), was machined near the HAZ to simulate the stress concentration of an under cut. The width of the heat affected zone was approximately 4.76 mm (3/16 in), located between weld and base plates. The specimen geometry is shown in Figure 7. A load of 320000 newtons (72000 lb) was applied at 0.089 m (3.5 in) on both sides of the center of the specimen to generate sufficient plastic strain at the notch root, while most of the specimen remained elastic. The strain was recorded periodically using Moire interferometry and a special high resolution grating technique; this was applied to the side surface near the notch root to obtain more accurate results. Strain fields were recorded periodically so that an entire strain vs. load history could be obtained and used later to compare with the finite element analysis. The

observation of crack initiation was performed on the notch root and side surface of the test specimen with the aid of a microscope and Moire interferometry. All testing mentioned above was conducted using a closed loop hydraulic tension-compression testing machine.

The yield strength of the HAZ was determined from micro hardness indentation tests. Due to the lack of uniformity of the material properties of the HAZ, the tests were conducted across its width. The average yield strength was found to be around 1241 MPa (180 Ksi).

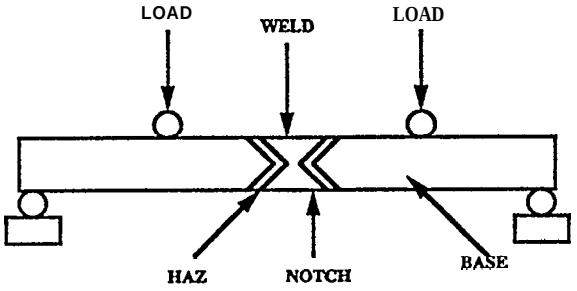

Figure 7. Schematic representation of the four point bend fatigue specimen. Dimensions are 0.58 m x 0.127 m x 0.051 m (23" x 5" x 2") (length x height x thickness).

NUMERICAL AND ANALYTICAL MODELING

It is usually quite difficult to accurately predict the notch root strain, as the effect of the surrounding elastic material on the notch root constraint is quite significant. In highly constrained sections the local root strains are difficult to predict. This constraint effect may affect fatigue crack initiation behavior (9). Current analytical notch root strain prediction models are either derived from plane stress, or plane strain situations. However, neglecting three-dimensional effects often yields unsatisfactory results. On the other hand, finite element techniques have the capability to model and analyze complex three-dimensional geometries without making unrealistic assumptions, which tend to oversimplify the actual loading conditions. It has keen demonstrated that, for fine-grained materials and moderately complex geometries, finite element predictions and experimental data show good agreement This is particularly true for the strain data along the loading direction (10). Two analytical models and the finite element method have been evaluated for their effectiveness in predicting the initiation of low cycle fatigue cracks at welded structural details in application.

Analytical Models

Two widely used analytical stress concentration strain prediction models widely used are the Neuber and Glinka relations. Their strain and stress relations are shown below:

$$K_\sigma \cdot K_\varepsilon = K_t^2 \qquad \text{Neuber (1)}$$

$$\frac{K_t^2 S^2}{2E} = \frac{\sigma^2}{2E} + \frac{\sigma}{n+1}\left(\frac{\sigma}{K}\right)^{1/n} \qquad \text{Glinka (2)}$$

where K_σ K_ε and K_t are stress, strain, and theoretical elastic stress concentration factors; S, σ, and n are the nominal stress, local stress, and Ramberg-Osgood hardening exponent respectively. Equation (2) is for plane strain situations.

Neuber's relation has proven to be very accurate in plane stress situations, such as the case of thin sheets with moderate strew concentrations. Glinka's model is an improved version based on the strain energy density for localized yielding. It has several modifications to handle plane stress and plane strain situations. Glinka's plane strain model has shown good agreement with experimental results for HY-80 steel in the past (10).

Numerical Models

Two- **and three-dimensional** finite element models were developed corresponding to the experimental notched specimens, so that the local stress-strain response could be computed and used to predict the crack initiation life. The solid models and finite element meshes were created using an interactive modeling software (11). A commercially available finite element code (12) was utilized for the computations. In order to accurately simulate the cyclic stress-strain response of the metallic materials, a two surface plasticity model was implemented in a user subroutine, and interfaced with the finite element program. This subroutine provided the code with the material behavior, returning to the main program the stress increment and instantaneous material stiffness for every strain increment supplied at each integration point in the model. The two surface theory is briefly described below with relevant references.

Two-Surface Incremental Plasticity Model

Plastic deformation occurs at material points where the stresses exceed the Mises yield condition. According to the flow theory of plasticity, the plastic strain rate, for an initially isotropic material, is given by Ziegler (13).

$$\dot{\varepsilon}_{ij}^{p} = (1 + H/3G)^{-1} n_{kl} \dot{\varepsilon}_{kl} n_{ij} \qquad (3)$$

where $\dot{\varepsilon}_{ij}$ is the total strain rate, n_{ij} is the direction of the outward normal to the yield surface at the current stress point, G is the elastic shear modulus of the material and His the instantaneous tangent modulus of

the stress-plastic strain curve. Plastic deformation causes the initial yield surface to translate and/or change size. In the analysis presented here, the center of the yield surface, α_{ii}, is assumed to translate kinematically according to Phillip's (14) hardening rule,

$$\dot{\alpha}_{ij} = \dot{\sigma}_{ij} \tag{4}$$

The size of the yield surface is assumed to remain fixed.

During cyclic loading, the plastic tangent modulus, H, varies nonlinearly with stress (or plastic strain). Here, His evaluated from the two-surface model proposed by Dafalias and Popov (15). This approach uses abounding surface which is an isotropic expansion of the yield surface. Initially the two surfaces are coaxial. During plastic straining the center of the bounding surface, β_{ij}, translates kinematically in the resultant direction of α_{ij} and μ_{ij}, (Figure 8). The unit vector μ_{ij} is along the line connecting the current stress point s and a corresponding point S on the bounding surface, both points having parallel outward normals. The rate of translation is given by

$$\dot{\beta}_{ij} = \dot{\alpha}_{ij} - \left(1 - \frac{H_0}{H}\right) \frac{\dot{\sigma}_{mn} n_{mn}}{\mu_{kl} n_{kl}} \mu_{ij} \tag{5}$$

where H_o is the asymptotic tangent modulus of the material's uniaxial response.

The instantaneous tangent modulus H is a function of the relative position of the two surfaces. It is computed from the formula

$$H = H_0 + h \frac{\delta}{(\delta_{in} - \delta)} \tag{6}$$

where δ is the distance between s and $\bar{s}$:

$$\delta = \sqrt{(\bar{\sigma}_{ij} - \sigma_{ij})(\bar{\sigma}_{ij} - \sigma_{ij})} \tag{7}$$

and n is a material property. The distance δ_{in} is the value of δ at the onset of yielding. Equation (6) indicates that when

$$\begin{aligned} \delta &= \delta_{in}, \qquad H = \infty \\ \delta &= 0, \qquad H = H_o \end{aligned} \tag{8}$$

For a uniaxial test the two-surface model leads to the scheme indicated in Figure 9. The parameters H_o, h, and the size of the bounding surface must be evaluated from the uniaxial experiments on the material of interest

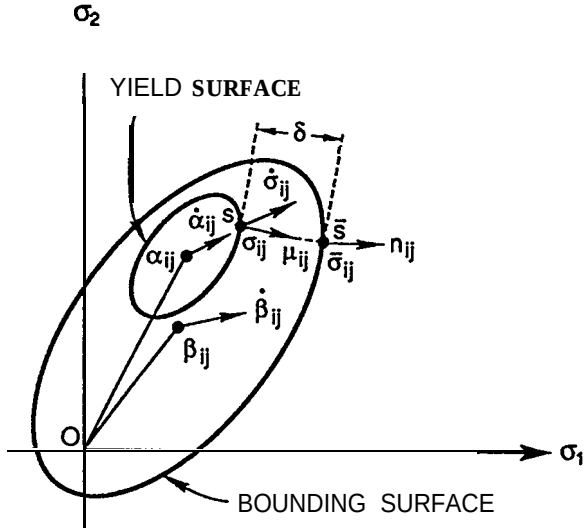

Figure 8. Schematic of the yield and bounding surfaces and their motion during plastic flow.

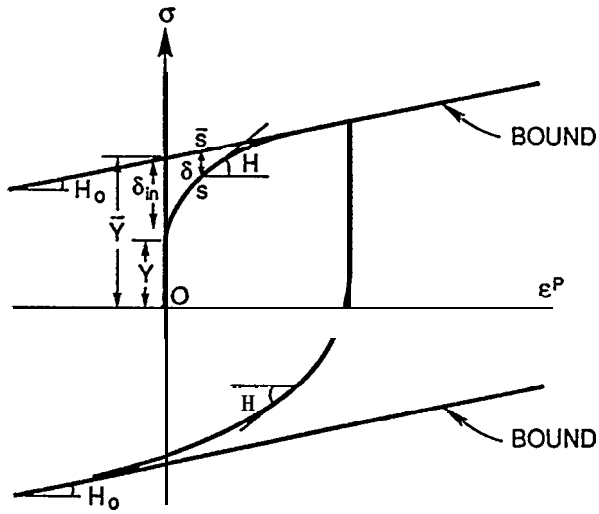

Figure 9. Evaluation of parameters from a uniaxial test for the finite element model.

Results

A three-dimensional finite element model of a 12.7 mm (0.5 in) thick double circular notched plate of HY-80 steel, with a notch root radius of 4.7 mm (0.185 in) and a width of 25.4 mm (1.0 in), was created. The purpose of this model was to evaluate the accuracy and validity of the two-surface plasticity theory in problems with high localized stress concentrations. Taking advantage of the symmetry conditions, only one eighth

of the actual specimen was modeled. Appropriate boundary conditions were applied to reflect the symmetry. The finite element mesh is shown in Figure 10. Three dimensional 20-node brick elements were used with reduced integration (8 integration points per element). The mesh comprises of a total of 721 elements, with the maximum number of elements near the notch root, where the steepest gradients exist. The material properties used for this simulation are given in TabIe II. The plasticity parameters correspond to the stabilized cycle of an experimental loading sequence on HY-80 Steel (10).

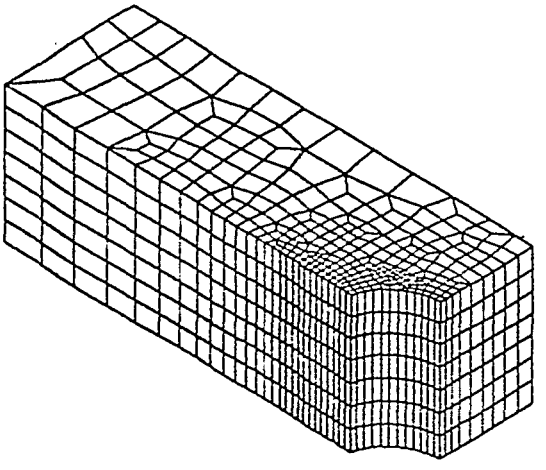

Figure 10. Three-dimensional finite element model of a 12.7 mm thick double circular notched plate (notch root radius 4.7 mm,width 25.4 mm).

The notch root strains along the loading direction from the finite element analysis have been plotted in Figure 11. They are compared with experimental data (10) obtained at the root of the notch using an interferometric strain/displacement gage (ISDG) (16) strain measurement system with a gage length of 100 micrometers. Very good agreement is seen between the finite element analysis and experimental results, except at the end of the compression region, probably due to some sliding between the specimen ends and the grips, causing a slight rotation of the specimen. The interference pattern may lose its normality, which is required for an accurate measurement however, this discrepancy is minor, as can be seen in the figure. The satisfactory results obtained using the two-surface cyclic model provided confidence to conduct the finite element analysis for other notch geometries and material combinations. Reference (10) indicates that Glinka's plane strain model showed good agreement with experimental data, while Neuber's relation underestimated the strains due to its plane stress assumption.

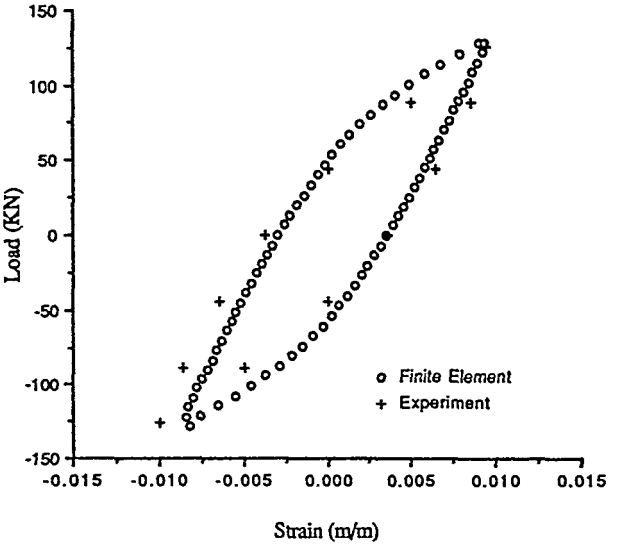

Figure 11. Finite element and experimental load vs. notch root strain curve from HY-80 double circular notched plate.

Cylindrical notched specimens were modeled with quadrilateral, axisymmetric, eight node elements. The dimensions of the models corresponded to those of the experimental specimens. Two notch root radii of 0.635 mm (0.025 in) and 0.381 mm (0.015 in) were used. Due to the symmetric nature of the specimen geomerry, only a quarter model was analyzed, with suitable boundary conditions. A typical finite element mesh is shown in Figure 12. Each mesh is comprised of 452 elements. Uniform surface pressure loads were applied on the unnotched end of the model. Materital properties for the

Material Property	HY-80 steel	HY-100 steel	HY-1OO Weld Metal	HAZ
Young's Modulus, E (GPa)	190.02	189.26	197.12	*200.02*
Poisson's Ratio, v	0.29	*0.3*	*0.295*	*03*
Yield Stress, Y (MPa)	299.92	330.95	159.96	1241.06
Tangent Modulus, (MPa)	7000.0	16750.0	*9000.O*	
Bound. Surf. radius (MPa)	510.0	600.0	490.0	
Hardening Param., h (GPa)	95.0	102.25	150.03	

Table II Material properties of HY-80 steel, HY-1OO steel, HY-100 weld metal and HAZ.

weld material were found from the uniaxial cyclic tests on the hourglass shaped specimens described earlier. The parameters used were for the stabilized cycle; they appear in Table II.

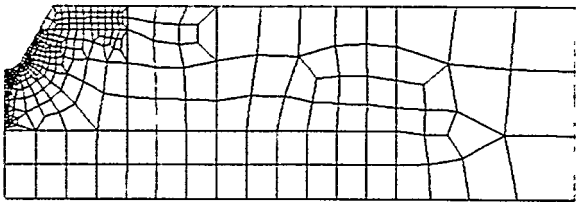

Figure 12. Finite element mesh of a notched cylindrical fatigue specimen.

The overall load versus notch root strain obtained from the finite element analysis has been plotted in Figure 13. The notch tip elastic stress concentration factors, K_t, were found to be 2.68 and 3.39 for radii 0.635 mm (0.025 in) and 0.381 mm (0.015 in) respectively. The finite element results were also compared with Glinka and Neuber strain prediction models, as shown in Figure 14. As can be seen here, the Glinka plane strain model, using the strain energy density concept, yielded excellent agreement with finite element analysis, while the Neuber relation loses its accuracy when higher plasticity and notch constraint are present. A comparison of the experimental and predicted fatigue lives is graphically represented in Figure 15.

Two- and three-dimensional finite element models of the four point bend fatigue specimen described earlier were also created. The model contains an HAZ thickness of 4.76 mm (3/16 in), between the weld metal and base metal, as shown in Figure 7. All other dimensions of the model correspond to those of the experimental specimen. Due to non-symmetry of the model, 760 8-node elements with 3003 nodes were needed for the two-dimensional model, and 154420-node elements with 6446 nodes for the three-dimensional model. The mesh used for either model is drawn in Figure 16. The loading applied was O to tension (R = 0) using nodal forces 0.089 m (3.5 in) from the center. Since the thickness of the four point bend specimen was 0.051 m (2.0 in), the notch produced near plane strain conditions so that the two-dimensional plane strain model yielded reasonable results. Material properties for HY-100 steel and the base metal are given in Table II. It was found that plastic deformation was localized at the notch tip and throughout the loading history; both the base metal and H&Z remained elastic.

Figure 17 shows experimental and numerical notch root strains plotted against load for the four point bend specimen. The experimental strains were recorded

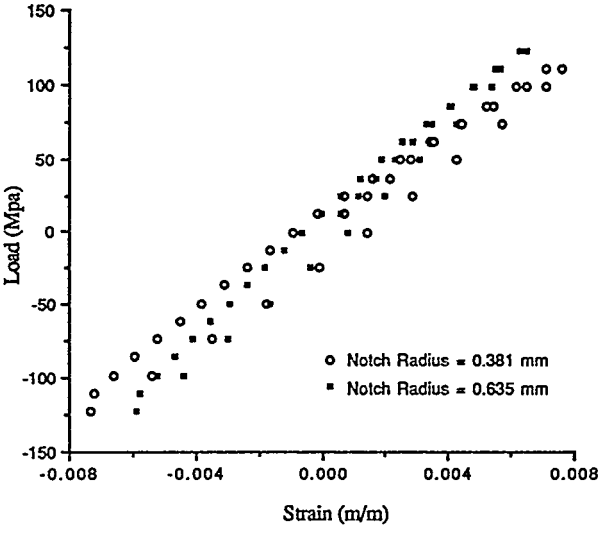

Figure 13. Overall load vs. notch root strain from finite element analysis of notched cylindrical fatigue specimens.

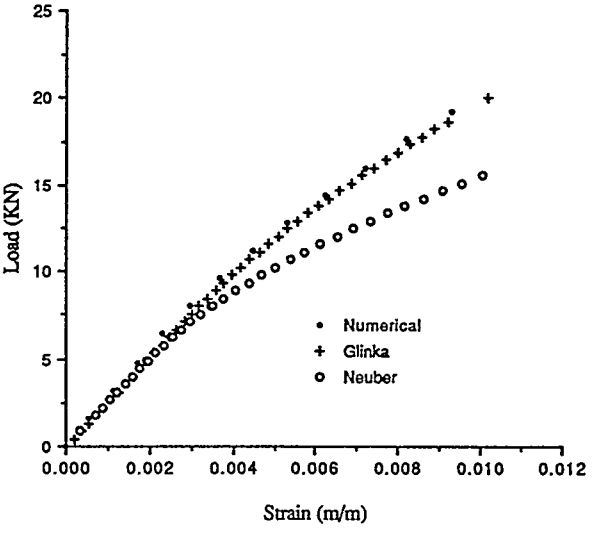

Figure 14. Notch root strain comparisons between finite element and analytical models for cylindrical notched specimens (notch root radius = 3.81 mm, notch depth =2.12 mm).

using Moire interferometry techniques. The agreement between the two is seen to be very good in the elastic range, however during plastic deformation the finite element predictions underestimate the actual strains. The numerical life prediction is compared with experimental results in Figure 15. The computed data points lie close to the 45 degree line, indicating fairly good accuracy of the numerical scheme.

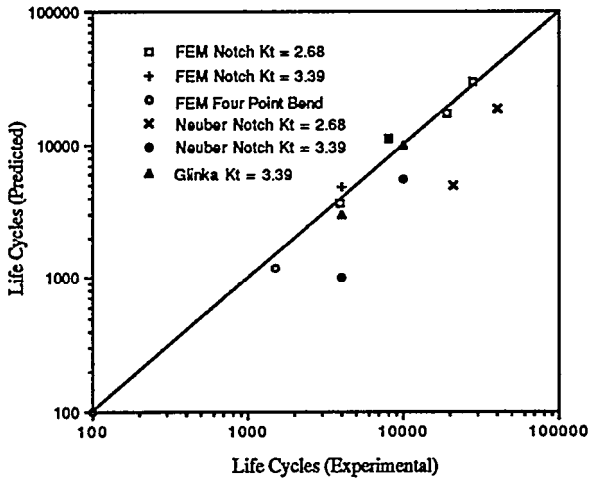

Figure 15. Comparison of experimental and predicted fatigue lives.

DISCUSSION AND CONCLUSIONS

The crack initiation life predicted by the finite element analyses and the Glinka and Neuber models were compared for their accuracy with experimental data as shown in Figure 15. The Glinka model captures the effect of constraint due to the presence of the sharp notch, while Neuber's relation is overly conservative in prediction of the crack initiation life of HY-100 under-matched welds, the finite element method, albeit the most expensive, provides the most reliable and accurate predictions of strain distribution to assess the crack initiation life. Glinka's prediction of the notch root strain works well for sharp notches and high stress concentrations, that is, when high constraints exist. The plastic zone surrounding the notch tip is relatively small. However, this is not true for Neuber's relation, which is based on the plane stress (less constraint) assumption. In general, Glinka's relations demonstrate better predictive capabilities for local strains than Neuber's relation, as is seen in Figure 14. The simplicity of calculating notch root strains with this method offers designers quick, inexpensive, and reasonably accurate results.

The baseline fatigue crack initiation and failure life obtained from smooth cylindrical specimens transverse to and along the weld are shown in Figure 5. Comparisons were also made between HY-130, HY-80 and HY-100 base metals. The differences between base and weld metal data are mom significant at higher loads. It is possible that due to the ductility of the weld, which has the lowest yield strength and a higher fracture toughness, the small fatigue crack propagation rate is lower than that of the base plate. At low load levels, fatigue controlled crack propagation resumed and the crack initiation behavior for the base metal and its weld became similar.

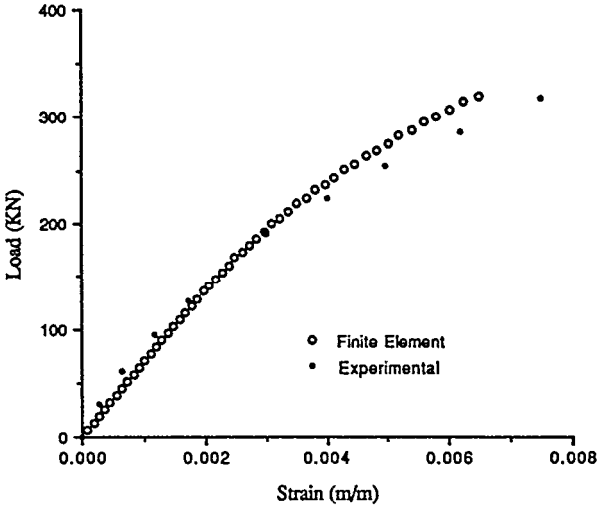

Figure 17. Experimental and finite element load vs. strain curve for a notched four point bend specimen near the notch tip.

The undermatched weldment of HY-100 steels shows similar baseline fatigue crack initiation life, although its yield strength is much lower than other HY series materials. More scatter was observed within the notched specimens than the smooth specimens. It must be noted that the grain size is quite large compared to the notch radius. The anisotropy at the notch root surface may be another contributor for the scatter of

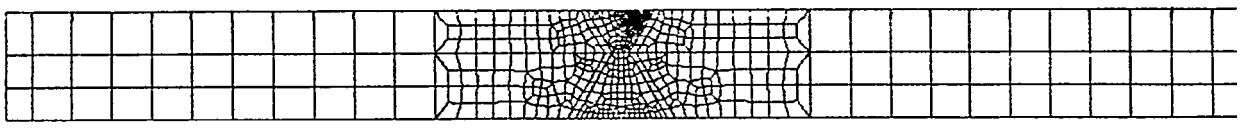

Figure 16. Finite element mesh of four-point bend fatigue specimen.

the tested results. Also, due to notch constraint effect, there is a build-up of multiaxial stress in the vicinity of the notch root. A best fit for the data set was found to obtain a single crack initiation or failure curve, which was then used in the finite element predictions. The finite element predicted crack initiation life of the four point bend fatigue specimen, using the stress-strain curves derived from hardness test, was reasonably close to the experimental results.

The results obtained from the modeling effort in this study demonstrated the effectiveness of the finite element method, and the two surface plasticity model, to predict the fatigue life of test specimens. The success of the analyses provides confidence to apply similar modeling techniques to structural components with more complex geometries. The experimental baseline fatigue crack initiation and failure life data can be used with the strain predictions from the numerical models to determine the life of the structural components.

ACKNOWLEDGEMENTS

This work was conducted by the National Center for Excellence in Metalworking Technology (NCEMT), operated by Concurrent Technologies Corporation, under contract to the U.S. Navy as part of the Navy's Manufacturing Technology Program. NCEMT is pleased to acknowledge the contributions of J.B. Sickles of David Taylor Model Basin, Carderock Division of the Naval Surface Warfare Center (CDNSWC), and E.J. Czyryza, Annapolis Detachment CDNSWC. Special thanks are due to Dr. Robert Czarnek and Dr. Shin-Yuan Lin for providing

REFERENCES

1. Ellingwood, Bruce R. and Lomacky Oles, "Analytical Evaluation of Low-Cycle Fatigue Behavior of HY-130 Steel Baseplate and Welds: Naval Ship Research and Development Center, Report 4490,1974.

2. Czyryca, E. J. and Davis, D. A., "Low-Cycle Corrosion Fatigue Crack Initiation and Growth in HY-100 Steel Weldments," David W. Taylor Naval Ship Research and Development Center, DTNSRDC/SME83/64,

3. Neuber, H., "Theory of Stress Concentration for Shear-Strained Prismatical Bodies with Arbitrary Nonlinear Stress-Strain Law: Journal of Applied Mechanics, v. 28, pp. 544-550,1961.

4. Glinka, G., "Energy Density Approach to Calculation of Inelastic Strain-Stress Near Notches and Cracks: Engineering Fracture Mechanics, v. 22, pp. 485-508,1985.

5. Wang, K. C., Shah, R. S., Yuan, D., Kleinosky, M. J., "Low Cycle Fatigue Crack Initiation Life Assesment of HY-100 Undermatched Weld," 34th AIAA/A SME Structures. Structural Dynamics. and Materials Conference.AdalItive Structures Forum, Part 4, pp. 2371-2377, La Jolla, CA, April 19-22, 1993.

6, Wang, K C., Shah, R. S., Kleinosky, MJ., "Low Cycle Fatigue Crack Initiation Life Assessment of HY-100 Undermatched Weld and HAZ," 1993 SEM "50th Anniversary" Spring Congerence on Experimental Mechanic, Dearborn,MI (June7-9, 1993).

7. Crews, J. H. and Hardrath, H. F., "Companion Specimen Method," Experimental Mechanics, V. 23, pp. 313-320, 1966.

8. ASTM E606-80, "Standard Recommended Practice for Constant-Amplitute Low Cycle Fatigue Testing," Annual Book of ASTM Standards, Section 3, v. 3.01,1988.

9. Krempl, E., "The Influence of State of Stress on Low Cycle Fatigue of Structural Material -- A Literature Survey and Report" ASTM STP 770,1980.

10. Sharpe, W. N., Jr., Yang, C. G. and Tregoning, R. L., "An Evaluation of the Neuber and Glinka Relations for Monotonic Loading," Journal of Applied Mechanics, v. 59, pp. 560-566,1992.

11. I-DEAS User's Manual, Structural Dynamics Research Corporation, Milford, Ohio, 1990.

12. ABAQUS User's Manual, Hibbit, Karlsson and Sorensen Inc., Providence, Rhode Island, 1989

13. Ziegler, H., "A Modification: of Prager's Hardening Rule," Quarterly of Applied Mathematics, v. 17, pp. 55-65,1959.

14. Phillips, A., Liu, C. S. and Justusson, J. W., "An Experimental Investigation of Yield Surfaces at Elevated Temperatures," Mechanica v. 14, pp. 119-146,1972.

15. Dafalias, Y.F. and Popov, E.P., "Plastic Internal Variables Formalism of Cyclic Plasticity: ASME Journal of Applied Mechanics, v. 43, pp. 147-157,1976.

16. Sharpe, W. N., Jr. and Wang, K. C., "Evaluation of a Modified Neuber Relation," Journal of Engineering Materials and Technology, v. 113,1991.